doi:10.3788/gzxb20174602.0229001

双峰分布颗粒体系的多角度动态光散射数据反演

徐敏[1]，申晋[1]，朱新军[2]，THOMAS John C[1,3]，
CLEMENTI Luis A[4]，VEGA Jorge R[4]
(1 山东理工大学 电气与电子工程学院，山东 淄博 255049)
(2 天津工业大学 电气工程与自动化学院，天津 300387)
(3 *Group Scientific Pty Ltd*，23 *Pine Lodge Crescent*，*Grange*，*SA* 5022，*Australia*)
(4 *Institute of Technological Development for the Chemical Industry* (*INTEC*，
UNL-CONICET)，*Güemes* 3450，3000 *Santa Fe*，*Argentina*)

摘 要：采用多角度动态光散射和加权正则化反演方法，对 4 组模拟的双峰分布颗粒体系(100/600 nm，200/600 nm，300/600 nm 和 350/600 nm)分别选取 1、3、6 和 10 个散射角进行测量.粒度反演结果表明，采用加权正则化方法反演双峰颗粒体系的多角度动态光散射测量数据，可获得峰值位置比小于 2∶1 且含有大粒径(>350 nm)颗粒的双峰颗粒粒度分布.采用标准聚苯乙烯乳胶颗粒进行实测的结果验证了这一结论.得到含大粒径颗粒的双峰粒度分布反演结果的原因在于，多角度动态光散射能提供更多的大粒径颗粒的粒度信息，加权正则化反演方法能减少测量数据中的噪声，因而多角度动态光散射测量数据的加权反演能实现峰值位置比小于 2∶1 且含有大粒径颗粒的双峰颗粒体系的测量.

关键词：动态光散射；粒度分布；加权约束正则化；峰值位置比；吉洪诺夫正则化
中图分类号：TN911.74　　**文献标识码**：A　　**文章编号**：1004-4213(2017)02-0229001-12

Recovery of Bimodal Particle Size Distributions with Multiangle Dynamic Light Scattering

XU Min[1]，SHEN Jin[1]，ZHU Xin-jun[2]，THOMAS John C[1,3]，CLEMENTI Luis A[4]，VEGA Jorge R[4]
(1 *School of Electrical and Electronic Engineering*，*Shandong University of Technology*，
Zibo，*Shandong* 255049，*China*)
(2 *The Key Laboratory of Advanced Electrical Engineering and Energy Technology*，
Tianjin Polytechnic University，*Tianjin* 300387，*China*)
(3 *Group Scientific Pty Ltd*，23 *Pine Lodge Crescent*，*Grange*，*SA* 5022，*Australia*)
(4 *Institute of Technological Development for the Chemical Industry*
(*INTEC*，*UNL-CONICET*)，*Güemes* 3450，3000 *Santa Fe*，*Argentina*)

Abstract: By using the multi-angle dynamic light scattering measurement and the weighted constrained regularization method, the four groups simulated particle systems with bimodal distribution(100/600 nm, 200/600 nm, 300/600 nm, 350/600 nm) were measured by selecting one, three, six and ten scattering angles respectively. The results of inversion of size distribution show that, by using the weighted constrained regularization method to inverse the multi-angle dynamic light scattering data of the particle

Foundation item: The National Natural Science Foundation of China (No. 61205191), the Natural Science Foundation of Shandong Province (Nos. ZR2014FL027, ZR2015FL034)
First author: XU Min(1990—), male, M. S. degree candidate, mainly focuses on dynamic light scatting technology. Email: minxu_90@yahoo.com
Supervisor(Contact author): SHEN Jin(1962—), male, professor, Ph. D. degree, mainly focuses on photoelectric precision measurement. Email: shenjin@sdut.edu.cn
Received: Oct. 9, 2016; **Accepted**: Dec. 1, 2016

systems with bimodal distribution, the bimodal particle size distributions with a peak position ratio less than 2∶1 and containing large particles(>350 nm) can be attained. This conclusion was verified by the measurement results of the standard polystyrene latex particles. The reason to attain the bimodal particle size distributions of the large particles is that, the multi-angle dynamic light scattering can provide more particle size information of large particles, the weighted constrained regularization inversion method can reduce the noise of the measurement data. Therefore, the weighted inversion of the multi-angle dynamic light scattering measurement data can achieve the measurement of the bimodal particle systems with a peak position ratio less than 2∶1 and containing large particles.

Key words: Dynamic light scattering; Particle size distribution; Weighted constrained regularization; Peak position ratio; Tikhonov constrained regularization

OCIS Codes: 290.0290; 290.5820; 290.5850; 120.5820

0 Introduction

The Particle Size Distribution (PSD) of polymer latex is an important morphological characteristic that determines the processability and end properties of the material[1]. Dynamic Light Scattering (DLS), as a popular technique for PSD determination of particles in the submicrometer range, has been widely applied in chemistry, medical, aerospace, environmental and other fields[2]. In DLS technique, the PSD can be obtained by recovering the Autocorrelation Function (ACF) of the light intensity. The inversion of ACF data is an inherently difficult problem in DLS measurements. It involves the inversion of a Fredholm integral of the first kind which is a typical ill-posed problem. The error involved in this inversion would make it particularly difficult to reliably recover bimodal PSDs when the peak position ratio is less than 2∶1. So many inversion algorithms have been proposed to address this situation. Multiangle DLS (MDLS) is a common method to improve the accuracy of the inversion results.

In 1987, Cummins and Staples[3] used two-angle DLS and showed that MDLS has advantages over single-angle DLS for the recovery of bimodal PSDs. In 1995, Bryant and Thomas[4] proposed and demonstrated that combining MDLS data with high quality Static Light Scattering (SLS) data, and analyzing the data simultaneously further improved the accuracy of PSD recovery. In their approach the Mie scattering function was used to weight ACF data in the analysis. Subsequently, Bryant et al[5]. showed that the same improvement could be achieved by re-iteratively generating the SLS data during PSD analysis. This had the great advantage of removing the requirement for separate high-quality SLS measurements making the measurements faster and also accessible to those without high quality goniometer systems to perform the SLS. Vega et al.[6] proposed a recursive least-squares method to estimate the weighting coefficients using the complete ACF measurement and a regularization parameter. Liu et al.[7] developed an iterative recursion method for obtaining the required intensity weighting and, using single-angle, three-angle, six-angle and nine-angle DLS, verified the relationship between the inversion accuracy and the number of scattering angle used in MDLS.

In the above methods, Constrained Regularization (CR) techniques are demonstrated to be effective inversion tools. However, these CR techniques are affected by the noise in ACF data and this does affect the inversion and PSD recovery[8]. For bimodal samples with a PSD with peak position ratio less than ~2∶1, or for samples where the ACF data has a low Signal-to-Noise Ratio (SNR), it is very difficult to obtain high inversion accuracy both in single-angle DLS and multi-angle DLS[7]. In order to reduce the adverse effects of the noise mixed in ACF data, Zhu et al.[9] proposed a Weighted Constrained Regularization (WCR) method and applied it in the single-angle DLS technique. The results confirmed that this method can improve the accuracy of the PSD recovery for bimodal samples with peak position ratio less than 2∶1 in the range of particle size less than 350nm which is usually called small particles. In the large particles (>350nm) range, it is still a difficult problem to obtain an accurate inversion and PSD recovery for bimodal samples with peak position ratio less than 2∶1. In this paper, we used WCR method to process the MDLS data for this kind of PSD. The results show that we can attain accurate PSD recovery for a bimodal PSD with peak position ratio less than 2∶1 containing the large particles (>350nm). Four simulated and two experimental ACF data sets were used to test the performance of the WCR method for

M-angle DLS measurements (M=1, 3, 6, 10).

1 The theory of MDLS measurement

The MDLS measurement is implemented by Photon Correlation Spectroscopy (PCS) technique, and ACF of light scattered by particles undergoing Brownian motion is collected at different scattering angles. In general, ACF of the scattered light intensity is given by

$$G_{\theta_r}^{(2)}(\tau) = \langle i_{\theta_r}(t) i_{\theta_r}(t+\tau) \rangle = \lim_{T_0 \to \infty} \frac{1}{T_0} \int_0^{T_0} i_{\theta_r}(t) i_{\theta_r}(t+\tau) \mathrm{d}t \tag{1}$$

where, $G_{\theta_r}^{(2)}(\tau)$ is ACF of scattered light intensity at scattering angle θ_r, $i_{\theta_r}(t)$ is the scattered light intensity, T_0 is the total analysis time and τ is the sampling time (delay time). In discrete form, Eq. (1) becomes

$$G_{\theta_r}^{(2)}(\tau_j) = \lim_{N \to \infty} \sum_{k=1}^{N} i_{\theta_r}(\tau_k) \cdot i_{\theta_r}(\tau_{k+j}) / N \tag{2}$$

where, $G_{\theta_r}^{(2)}(\tau_j)$ is the discrete form of $G_{\theta_r}^{(2)}(\tau)$, τ_j is the discrete delay time, and N is the total number of light intensity samples. And ACF of the scattered light intensity is related to the normalized ACF of the electric field, $g_{\theta_r}^{(1)}(\tau_j)$, through the Siegert relationship[10]

$$G_{\theta_r}^{(2)}(\tau_j) = B(1+\beta|g_{\theta_r}^{(1)}(\tau_j)|^2) \qquad (\theta_r = \theta_1, \theta_2, \cdots, \theta_m; j = 1, 2, \cdots, M) \tag{3}$$

where, B is the baseline of ACF, $\beta(\leqslant 1)$ is an instrumental coherence constant, and M is the total number of channels or points of ACF measured at the scattering angle θ_r, m is the number of the scattering angles.

For a polydisperse system of particles, ACF of the field is represented by a weighted sum of exponentials as

$$g_{\theta_r}^{(1)}(\tau_j) = \sum_{i=1}^{N} \exp(-\Gamma(\theta_r, d_i) \cdot \tau_j) \cdot h_{\theta_r}(d_i) \tag{4}$$

where, d_i is the diameter of the spherical particles, $h_{\theta_r}(d_i)$ is the angular scattered intensity distribution of the particles and $\Gamma(\theta_r, d_i)$ is the exponential decay constant, which depends on the modulus of the scattering vector and the diffusion coefficient of the particles ($K(\theta_r)$ and $D(d_i)$).

The diffusion coefficient and diameter of the spherical particles are related by the Stokes-Einstein equation[10] as

$$D(d_i) = \frac{k_B T}{3\pi\eta d_i} \tag{5}$$

where, T is the absolute temperature of the medium, η is the viscosity of the dispersing medium, and k_B is the Boltzmann constant.

Thus, the decay constant can be calculated as

$$\Gamma(\theta_r, d_i) = K^2(\theta_r) \cdot D(d_i) = \left(\frac{4\pi n_m(\lambda_0) \cdot \sin(\theta_r/2)}{\lambda_0}\right)^2 \cdot \frac{k_B T}{3\pi\eta d_i} = \frac{16\pi \cdot k_B T \cdot n_m^2(\lambda_0) \cdot \sin^2(\theta_r/2)}{3\eta d_i \lambda_0^2} \tag{6}$$

where, λ_0 is the wavelength of the incident light, θ_r is the scattering angle and $n_m(\lambda_0)$ is the refractive index of the non-absorbing suspending medium. These parameters are related with $K(\theta_r)$.

The angular scattered intensity distribution of the particles, $h_{\theta_r}(d_i)$, is related to the PSD[11] by

$$h_{\theta_r}(d_i) = k_{\theta_r} C_{I_{\theta_r}}(d_i) f(d_i) \tag{7}$$

where, k_{θ_r} is an *a* priori unknown constant which is related to the scattering angle θ_r, and ensures the normalization of $h_{\theta_r}(d_i)$; $C_{I_{\theta_r}}(d_i)$ is the fraction of light intensity scattered by a particle with diameter d_i at scattering angle θ_r and is calculated through the Mie scattering theory[12-13], $f(d_i)(i=1,2,\cdots,N)$ is the discrete PSD which represents the number particle concentration in the range $[d_i, d_{i+1}]$ and N is the (chosen) total number of PSD points that are evenly spaced in the range $[d_{\min}, d_{\max}]$.

Normalization means, $\sum_{i=1}^{N} h_{\theta_r}(d_i) = 1$ and we can calculate the constant k_{θ_r} through Eq. (7) by

$$k_{\theta_r} = 1 / \sum_{i=1}^{N} C_{I_{\theta_r}}(d_i) f(d_i) \qquad (i = 1, 2, \cdots, N) \tag{8}$$

Substituting Eq. (6) and Eq. (7) into Eq. (4), we obtain the normalized field ACF as

$$\begin{aligned} g_{\theta_r}^{(1)}(\tau_j) &= k_{\theta_r} \sum_{i=1}^{N} \exp(-\Gamma(\theta_r, d_i) \cdot \tau_j) \cdot C_{I_{\theta_r}}(d_i) f(d_i) \\ \Gamma(\theta_r, d_i) &= \frac{16\pi}{3} \frac{k_B T}{\eta} \frac{n_m^2}{\lambda_0^2} \frac{\sin^2(\theta_r/2)}{d_i} \quad (\theta_r = \theta_1, \theta_2, \cdots, \theta_m; j = 1, 2, \cdots, M; i = 1, 2, \cdots, N) \end{aligned} \tag{9}$$

In vector notation we can write as

$$\boldsymbol{g}_{\theta_r}^{(1)}=k_{\theta_r}\boldsymbol{A}_{\theta_r}\boldsymbol{f}\qquad(\theta_r=\theta_1,\theta_2,\cdots,\theta_m)\tag{10}$$

where, $\boldsymbol{g}_{\theta_r}^{(1)}$ is a vector with elements $g_{\theta_r}^{(1)}(\tau_j)$ whose size is $M\times1$; f is a vector with elements $\boldsymbol{f}(d_i)$ whose size is $N\times1$; $\boldsymbol{A}_{\theta_r}$ is a kernel matrix whose size is $M\times N$ corresponding to the measured ACF at the scattering angle θ_r. The elements of $\boldsymbol{A}_{\theta_r}$ are given by

$$\begin{cases}\boldsymbol{A}_{\theta_r}(j,i)=\exp(-\Gamma(\theta_r,d_i)\tau_j)C_{I_{\theta r}}(d_i)\\ \Gamma(\theta_r,d_i)=\dfrac{16\pi}{3}\dfrac{k_{\mathrm{B}}T}{\eta}\dfrac{n_m^2}{\lambda_0^2}\dfrac{\sin^2(\theta_r/2)}{d_i}\end{cases}\qquad(j=1,2,\cdots,M;i=1,2,\cdots,N)\tag{11}$$

2 Inversion algorithms for MDLS measurement

To estimate PSD by MDLS, ACF data at different scattering angles θ_r, are treated as one set, and described by

$$g^{(1)}=\begin{bmatrix}g_{\theta_1}^{(1)}\\g_{\theta_2}^{(1)}\\\vdots\\g_{\theta_m}^{(1)}\end{bmatrix}=\begin{bmatrix}k_{\theta_1}A_{\theta_1}\\k_{\theta_2}A_{\theta_2}\\\vdots\\k_{\theta_m}A_{\theta_m}\end{bmatrix}f=k_{\theta_1}\begin{bmatrix}kk_{\theta_1}A_{\theta_1}\\kk_{\theta_2}A_{\theta_2}\\\vdots\\kk_{\theta_m}A_{\theta_m}\end{bmatrix}f\qquad(kk_{\theta_r}=k_{\theta_r}/k_{\theta_1},\theta_r=\theta_1,\theta_2,\cdots,\theta_m)\tag{12}$$

where, the constants k_{θ_1}, k_{θ_2}, $\cdots$, k_{θ_m} are the constant at the scattering angles θ_1, θ_2, $\cdots$, θ_m; kk_{θ_r} is a dimensionless weighting ratio given by the ratio of k_{θ_r} and k_{θ_1} in Eq. (12). We can simplify the form of Eq. (12) by

$$\boldsymbol{g}^{(1)}=k_{\theta_1}\boldsymbol{A}\boldsymbol{f}=\boldsymbol{A}^{k_{\theta_1}}\boldsymbol{f}\tag{13}$$

And then, we can calculate the PSD after the inversion of Eq. (13). However, the estimation of $\boldsymbol{f}$ from Eq. (13) is a typical ill-posed problem, usually requiring regularization techniques to obtain a reliable result. The goal of regularization techniques is to realize the inversion of Eq. (13) via a method which is robust, demanding as little information from the operator as possible, and requiring a short computational time. Constrained Regularization (CR) methods such as the constrained Tikhonov regularization method have shown good results[14]. The Tikhonov method is expressed as a constrained functional optimization problem by

$$M^{\alpha}(\boldsymbol{f},\boldsymbol{g}^{(1)})=\|\boldsymbol{A}^{k_{\theta_1}}\boldsymbol{f}-\boldsymbol{g}^{(1)}\|^2+\alpha\|\boldsymbol{L}\boldsymbol{f}\|^2\quad\text{s.t.}\quad f\geqslant0\tag{14}$$

The optimal solution of Eq. (14), $\boldsymbol{f}$, is the solution of Eq. (13). The constant α is the regularization parameter which controls the fair balance of accuracy and stability of the optimal solution, the matrix $\boldsymbol{L}$ is the regular matrix which makes the solution smooth, $\|\cdot\|$ is the Euclidean norm and $\|\boldsymbol{L}\boldsymbol{f}\|^2$ is the penalty factor which ensures the solution is stable.

Analyzing Eq. (14), we find that the CR methods are relatively immune to the larger noise due to the baseline error and square root extraction. This means the CR methods do not take into account the fact that all of the ACF data do not contribute signal information equally due to the noise differences in the ACF data at different lag time. To restrain the effect of large noise at different (long) lag times, we introduce a weighted CR method into the MDLS analysis expressed by

$$M_W^{\alpha}(\boldsymbol{f},\boldsymbol{g}^{(1)})=\|\boldsymbol{W}(\boldsymbol{A}^{k_{\theta_1}}\boldsymbol{f}-\boldsymbol{g}^{(1)})\|^2+\alpha\|\boldsymbol{L}\boldsymbol{F}\|^2\quad\text{s.t.}\quad f\geqslant0\tag{15}$$

where, $\boldsymbol{W}$ is a weighting matrix which can adjust the contribution of the ACF data $\boldsymbol{g}^{(1)}$ at different lag time τ_j. This can be expressed as $[W_{\theta_1},W_{\theta_2},\cdots,W_{\theta_m}]^{\mathrm{T}}$. W_{θ_r} is the weighting matrix of the ACF data whose size is $M\times M$, and has the form $W_{\theta_r}=\mathrm{diag}((w_{\theta_r})^{0.5})$ with the vector elements $(w_{\theta_r})^{0.5}$ on the main diagonal, where diag is the diagonal operator.

We can express the MDLS measurement (Eq. (12)) including the weighted CR as

$$\boldsymbol{g}_W^{(1)}=\begin{bmatrix}\boldsymbol{W}_{\theta_1}\boldsymbol{g}_{\theta_1}^{(1)}\\\boldsymbol{W}_{\theta_2}\boldsymbol{g}_{\theta_2}^{(1)}\\\vdots\\\boldsymbol{W}_{\theta_m}\boldsymbol{g}_{\theta_m}^{(1)}\end{bmatrix}=\begin{bmatrix}k_{\theta_1}\boldsymbol{W}_{\theta_1}\boldsymbol{A}_{\theta_1}\\k_{\theta_2}\boldsymbol{W}_{\theta_2}\boldsymbol{A}_{\theta_2}\\\vdots\\k_{\theta_m}\boldsymbol{W}_{\theta_m}\boldsymbol{A}_{\theta_m}\end{bmatrix}\boldsymbol{f}=k_{\theta_1}\begin{bmatrix}kk_{\theta_1}\boldsymbol{W}_{\theta_1}\boldsymbol{A}_{\theta_1}\\kk_{\theta_2}\boldsymbol{W}_{\theta_2}A_{\theta_2}\\\vdots\\kk_{\theta_m}\boldsymbol{W}_{\theta_m}\boldsymbol{A}_{\theta_m}\end{bmatrix}\boldsymbol{f}\qquad(kk_{\theta_r}=k_{\theta_r}/k_{\theta_1},\theta_r=\theta_1,\theta_2,\cdots,\theta_m)\tag{16}$$

Eq. (16) can be written in simplified form as

$$\boldsymbol{g}_W^{(1)}=k_{\theta_1}\boldsymbol{A}_W\boldsymbol{f}=\boldsymbol{A}_W^{k_{\theta_1}}\boldsymbol{f}\tag{17}$$

So the first term of Eq. (15) can be expressed as

$$\| \boldsymbol{W}(\boldsymbol{A}^{k_{\theta_1}}\boldsymbol{f}-\boldsymbol{g}^{(1)}) \|^2 = \| \boldsymbol{A}_W^{k_{\theta_1}}\boldsymbol{f}-\boldsymbol{g}_W^{(1)} \|^2 = \sum_{j=1}^{M\times m}[w_j(\boldsymbol{\alpha}_j\boldsymbol{f}-\boldsymbol{g}^{(1)}(j))]^2 \tag{18}$$

where, a_j is the j^{th} row of $\boldsymbol{A}^{k_{\theta_1}}$, w_j is the j^{th} element of the weighting matrix $\boldsymbol{W}$.

In this study, we choose the weighting matrix $\boldsymbol{W}_{\theta_r}$ of the ACF data $g_{\theta_r}^{(1)}$ as $W_{\theta_r}=\text{diag}(|g_{\theta_r}^{(1)}|^{Pr/2})$ which means that $w_{\theta_r-j}=|g_{\theta_r-j}^{(1)}|^{Pr}$. $|g_{\theta_r-j}^{(1)}|$ denotes the absolute value of $g_{\theta_r-j}^{(1)}$, and P_r is an adjustable parameter. In the following the performance of the weighted CR method of MDLS analysis is tested using simulated data and experimental data.

3 Simulated data

In this section, we investigate the performance of the weighted CR method for MDLS data analysis using simulated data. To simulate a more realistic bimodal PSD, we used a bimodal system of polydisperse particles, which was described in Eq. (19) by a combination of two PSDs from Johnson's S_B distribution[15].

$$f(d)=a\frac{\sigma_1}{(d_{\max}-d_{\min})\sqrt{2\pi}}[t(1-t)]^{-1}\exp\left\{-0.5\left[u_1+\sigma_1\ln\left(\frac{t}{1-t}\right)\right]^2\right\}+b\frac{\sigma_2}{(d_{\max}-d_{\min})\sqrt{2\pi}}\cdot \tag{19}$$
$$[t(1-t)]^{-1}\exp\left\{-0.5\left[u_2+\sigma_2\ln\left(\frac{t}{1-t}\right)\right]^2\right\} \qquad (a+b=1)$$

where, $t=(d-d_{\min})/(d_{\max}-d_{\min})$, μ_1, σ_1, μ_2, σ_2, a, b are distribution parameters, we can change these parameters to get different PSDs. d is the diameter of the particle, $d_{\min}$ and $d_{\max}$ are the maximum and minimum particle diameter, respectively, t is the normalized particle diameter. The intensity ACF without noise is obtained using Eq. (3) and Eq. (9). Four sets of PSD data were simulated with the parameters shown in Table 1 and then four sets of ACF data were simulated using the parameters shown in Table 2. What's more, d_1 and d_2 in the Table 2 is the diameters at the maximum of each peak.

Table 1 Properties of simulated bimodal polydisperse PSD data sets

Sample	μ_1	σ_1	μ_2	σ_2	a	b
AS	9.0	5.0	−4.2	3.8	0.35	0.65
BS	7.0	6.5	−4.2	3.8	0.38	0.62
CS	4.0	8.0	−7.5	7.0	0.45	0.55
DS	2.5	10.0	−7.9	7.0	0.46	0.54

Table 2 Properties of simulated ACF data sets for the bimodal polydisperse PSDs

Sample	d_1/nm	d_2/nm	$d_2:d_1$	Intensity ratio	Added noise
AS	112	608	5.4∶1	1∶1	3×10^{-3}
BS	200	608	3.0∶1	1∶1	3×10^{-3}
CS	304	600	2.0∶1	1∶1	3×10^{-3}
DS	352	608	1.7∶1	1∶1	3×10^{-3}

All of the ACF data are simulated with $k_B=1.3807\times10^{-23}$ J/K, $T=298.15$ K, $\eta=0.89$ cP, $n_m=1.3316$, $\lambda_0=632.8$ nm, $\theta_r=30°, 40°, 50°, \cdots, 140°$; $B=1$, and $\beta=0.7$; $d_{\min}=0.01$ nm; $d_{\max}=800.01$ nm; Number of Points is 100.

The simulated ACF data were made more realistic by adding Gaussian random noise with noise levels shown in Table 2. The noise was added using[8]

$$G_{\text{noise}\_\theta_r}^{(2)}(\tau_j)=G_{\theta_r}^{(2)}(\tau_j)+\delta\varepsilon(\tau_j) \qquad (\theta_r=\theta_1,\theta_2,\cdots,\theta_m;j=1,2,\cdots,M) \tag{20}$$

where, $G_{\text{noise}\_\theta_r}^{(2)}(\tau_j)$ is the unnormalized intensity ACF data with noise, $G_{\theta_r}^{(2)}(\tau_j)$ is the noise-free data, $\varepsilon(\tau_j)$ is the uncorrelated Gaussian random noise, and δ is the noise level.

Analysis of the simulated noisy ACF data was performed using the Tikhonov CR method and the WCR method for single-angle DLS, 3-angle DLS, 6-angle DLS and 10-angle DLS. Here, single-angle DLS was simulated at 90°; 3-angle DLS was simulated at 70°, 90° and 110°; 6-angle DLS was simulated at 30°, 50°, ⋯, 130°; 10-angle DLS was simulated at 30°, 40°, ⋯, 120°. The values of α are determined using the L-curve method[16]. The values of kk_{θ_r} are estimated using the iterative recursion method for MDLS[7]. And we judged the quality of the recovered PSDs using five index parameters: the peak positions, relative error

of peak positions, the intensity ratios of the components, the area ratios and a goodness-of-fit performance index V. The intensity ratios of the components were calculated as the ratios between the maximum heights of both peaks, while the area ratios were calculated as the ratios between the areas under both peaks. The goodness-of-fit performance index V is used to judge the quality of the recovered PSDs, which is defined as

$$V=\left\{\frac{\sum_1^K[f(d)-\hat{f}(d)]^2}{K}\right\}^{1/2} \tag{21}$$

where, $f(d)$ is the true simulated PSD and $\hat{f}(d)$ is the recovered PSD.

Figs. 1～4 show the PSDs recovered from the simulated bimodal data sets using the two analysis methods and Tables 3～6 give the corresponding peak positions, relative error of peak positions, the intensity ratios of the components, the corresponding area ratios and performance index V in the true and recovered PSDs.

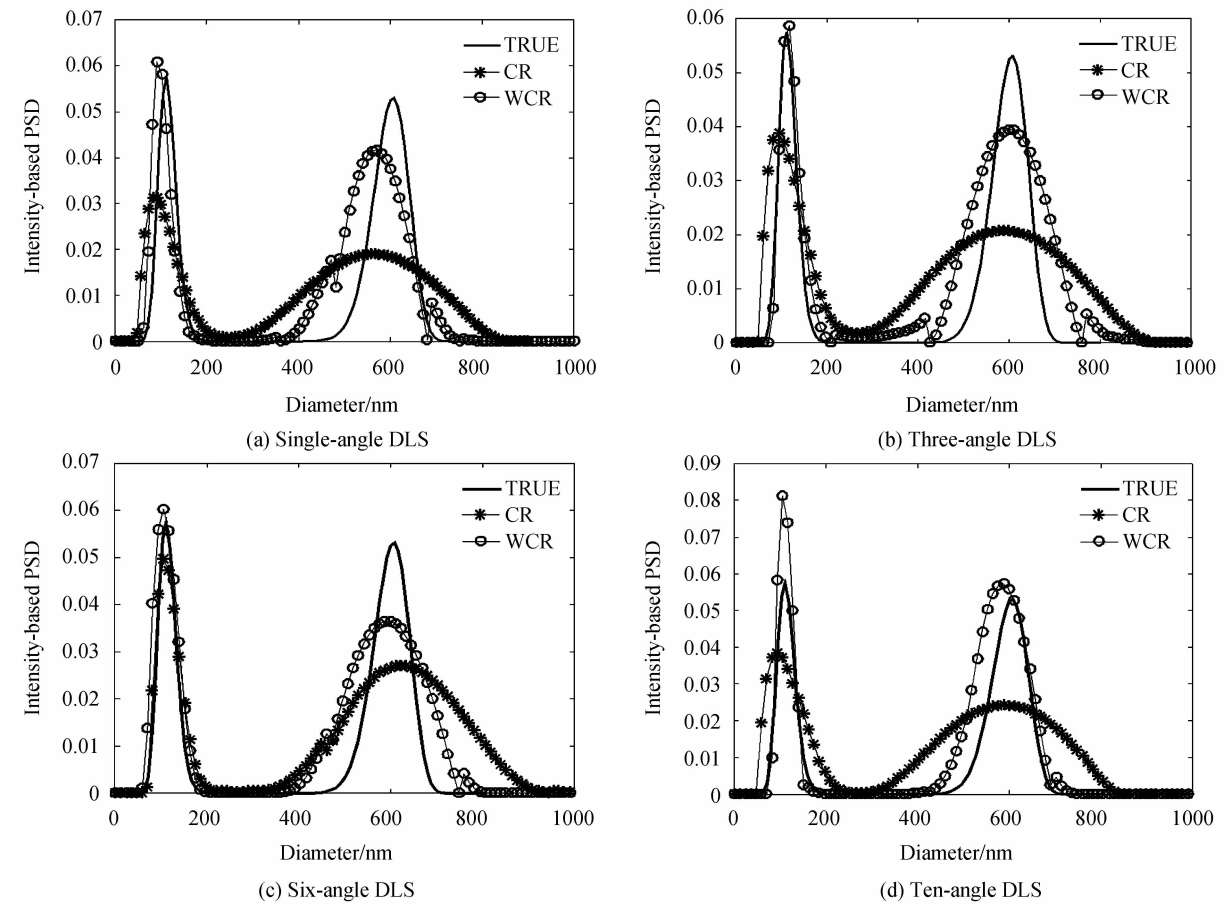

Fig. 1 Intensity-based PSDs recovered from sample AS using CR and WCR method (CR/WCR)

Table 3 Peak position, relative error of peak position, peak intensity ratio and peak area ratio of true and recovered PSDs for sample AS

			Peak position/nm	Relative error of peak position	Intensity ratio	Area ratio	V
True PSD			112/608	0.000/0.000	1.000∶0.925	1.000∶1.857	0
Recovered PSDs	1-angle DLS	CR	92/568	0.179/0.066	1.000∶0.609	1.000∶2.273	0.015
		WCR	92/571	0.179/0.061	1.000∶0.686	1.000∶2.238	0.024
	3-angle DLS	CR	94/588	0.161/0.033	1.000∶0.540	1.000∶1.980	0.021
		WCR	117/599	0.045/0.015	1.000∶0.673	1.000∶2.488	0.024
	6-angle DLS	CR	105/622	0.063/0.023	1.000∶0.546	1.000∶2.642	0.025
		WCR	105/599	0.063/0.015	1.000∶0.605	1.000∶1.970	0.021
	10-angle DLS	CR	94/599	0.161/0.015	1.000∶0.627	1.000∶2.011	0.022
		WCR	105/588	0.063/0.033	1.000∶0.708	1.000∶2.282	0.028

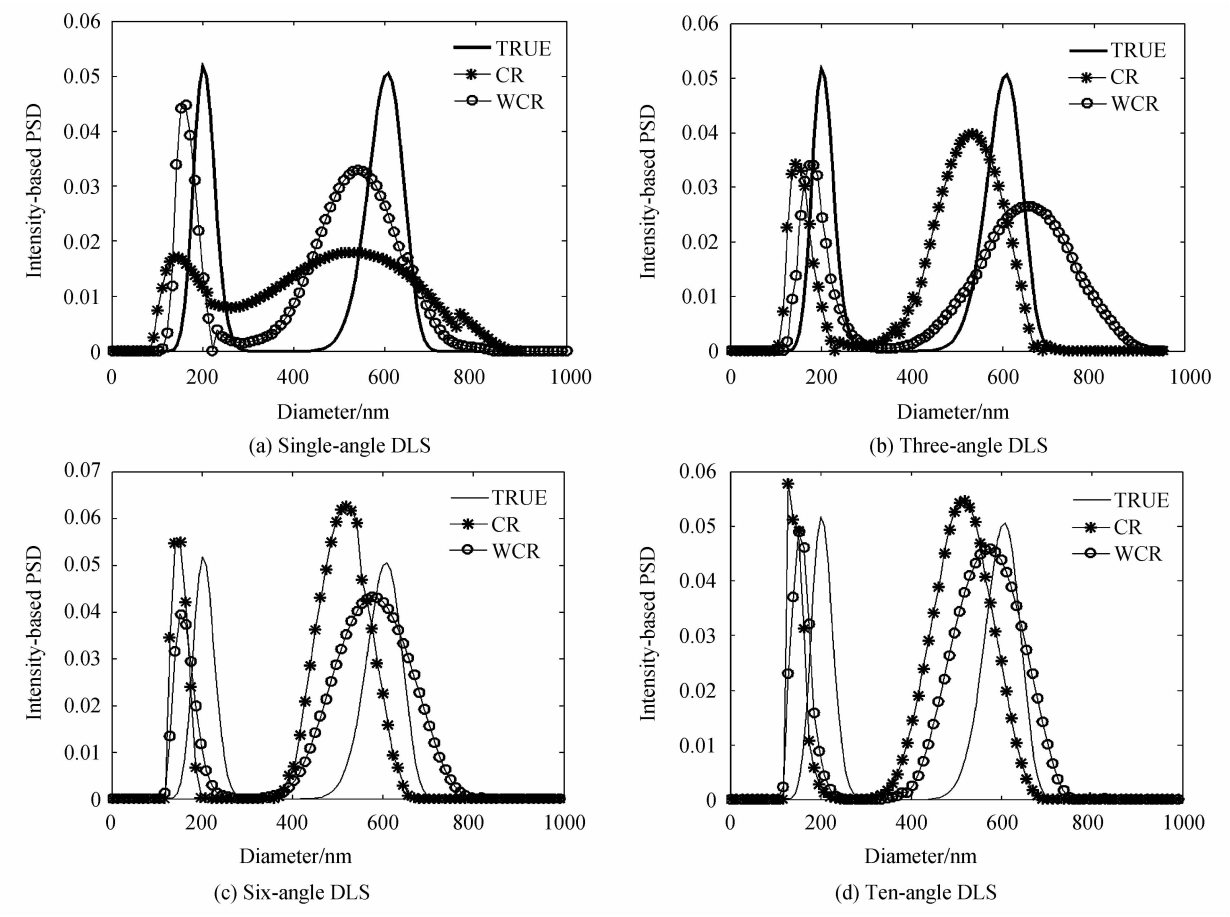

Fig. 2 Intensity-based PSDs recovered from sample BS using CR and WCR method (CR/WCR)

Table 4 Peak position, relative error of peak position, peak intensity ratio and peak area ratio of true and recovered PSDs for sample BS

			Peak position/nm	Relative error of peak position	Intensity ratio	Area ratio	V
	True PSD		200/608	0.000/0.000	1.000 : 0.977	1.000 : 1.632	0
Recovered PSDs	1-angle DLS	CR	146/532	0.270/0.125	1.000 : 1.059	1.000 : 3.170	0.017
		WCR	162/541	0.190/0.110	1.000 : 0.734	1.000 : 2.993	0.023
	3-angle DLS	CR	145/534	0.275/0.122	1.000 : 1.154	1.000 : 3.413	0.025
		WCR	182/656	0.090/0.079	1.000 : 0.778	1.000 : 2.596	0.015
	6-angle DLS	CR	151/519	0.245/0.146	1.000 : 1.140	1.000 : 3.569	0.029
		WCR	151/576	0.245/0.053	1.000 : 1.096	1.000 : 4.081	0.026
	10-angle DLS	CR	128/519	0.360/0.146	1.000 : 0.945	1.000 : 3.726	0.028
		WCR	151/588	0.245/0.033	1.000 : 0.935	1.000 : 3482	0.027

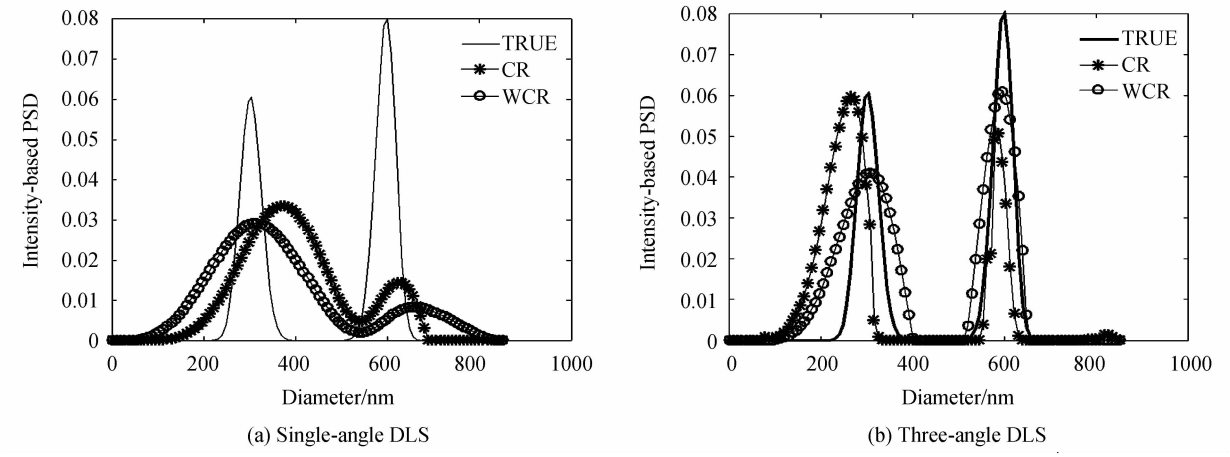

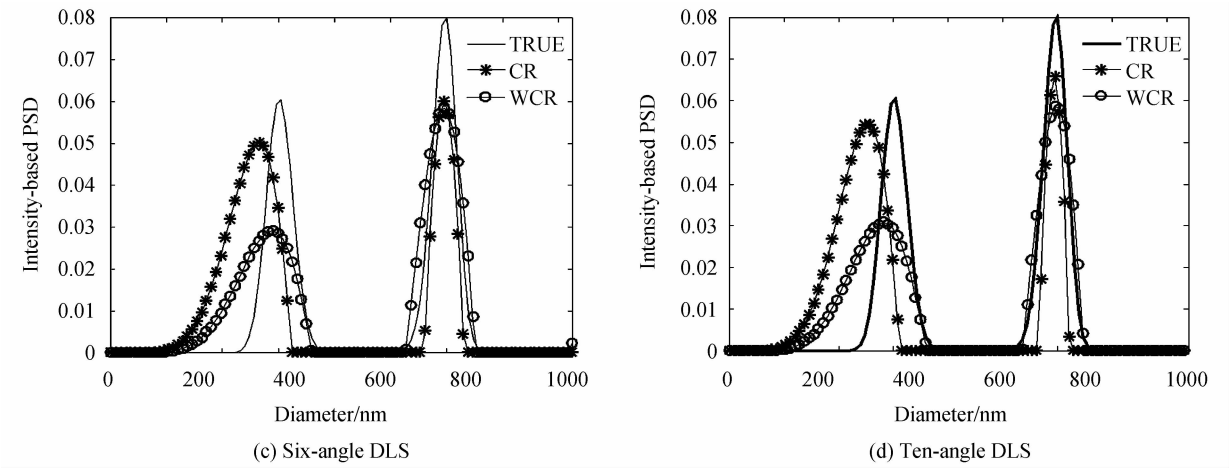

Fig. 3 Intensity-based PSDs recovered from sample CS using CR and WCR method (CR/WCR)

Table 5 Peak position, relative error of peak position, peak intensity ratio and peak area ratio of true and recovered PSDs for sample CS

			Peak position/nm	Relative error of peak position	Intensity ratio	Area ratio	V
	True PSD		304/600	0.000/0.000	1.000∶1.322	1.000∶1.222	0
Recovered PSDs	1-angle DLS	CR	367/638	0.207/0.060	1.000∶0.414	1.000∶0.198	0.018
		WCR	307/655	0.010/0.086	1.000∶0.291	1.000∶0.204	0.019
	3-angle DLS	CR	264/587	0.132/0.022	1.000∶0.848	1.000∶0.342	0.027
		WCR	307/596	0.010/0.007	1.000∶1.481	1.000∶0.846	0.019
	6-angle DLS	CR	265/596	0.128/0.007	1.000∶1.199	1.000∶0.555	0.025
		WCR	290/596	0.046/0.007	1.000∶2.010	1.000∶1.361	0.019
	10-angle DLS	CR	256/596	0.158/0.007	1.000∶1.210	1.000∶0.439	0.027
		WCR	256/598	0.158/0.003	1.000∶1.210	1.000∶1.112	0.019

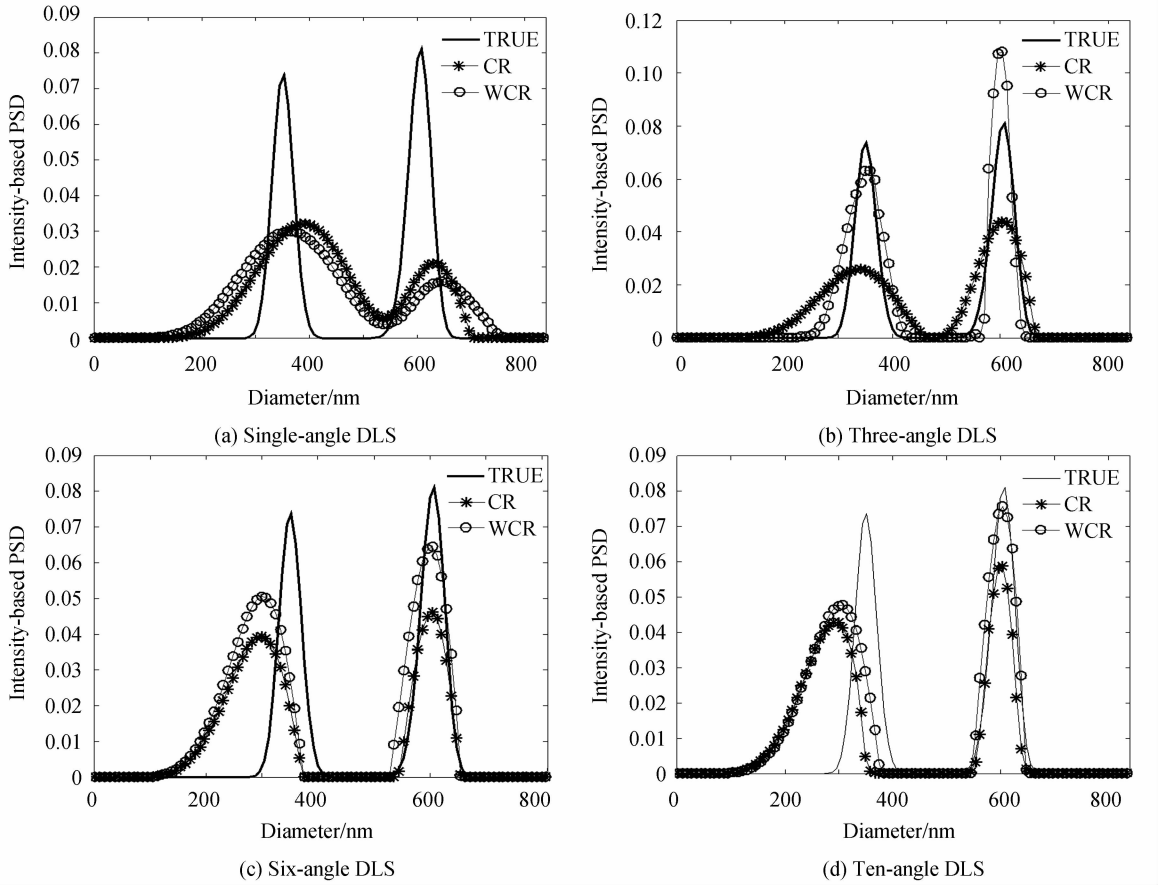

Fig. 4 Intensity-based PSDs recovered from sample DS using CR and WCR method (CR/WCR)

Table 6 Peak position, relative error of peak position, peak intensity ratio and peak area ratio of true and recovered PSDs for sample DS

			Peak position/nm	Relative error of peak position	Intensity ratio	Area ratio	V
True PSD			352/608	0.000/0.000	1.000 : 0.910	1.000 : 1.174	0
Recovered PSDs	1-angle	CR	384/630	0.091/0.036	1.000 : 0.654	1.000 : 0.341	0.017
	DLS	WCR	358/647	0.017/0.064	1.000 : 0.530	1.000 : 0.326	0.018
	3-angle	CR	341/604	0.031/0.006	1.000 : 1.700	1.000 : 1.000	0.019
	DLS	WCR	350/604	0.006/0.006	1.000 : 1.705	1.000 : 0.898	0.026
	6-angle	CR	299//604	0.151/0.006	1.000 : 1.170	1.000 : 0.698	0.025
	DLS	WCR	307/604	0.128/0.006	1.000 : 1.275	1.000 : 0.869	0.028
	10-angle	CR	290/604	0.176/0.006	1.000 : 1.372	1.000 : 0.670	0.027
	DLS	WCR	310/604	0.119/0.006	1.000 : 1.584	1.000 : 0.842	0.028

Examination of Fig. 1 and Table 3 shows that both CR and WCR method recover reliably two-component PSDs for Sample AS (112 nm/608 nm bimodal). For 1-, 3-, 6- and 10-angle data, WCR method recovers the peaks more accurately than CR method. In all cases the relative intensity of the peak at large sizes is closer to the expected peak intensity ratio of 1.000 : 0.925 by the WCR method than the CR method.

Fig. 2 and Table 4 show the PSD results obtained for Sample BS (200 nm/608 nm bimodal). It can be seen that CR method does not resolve two obvious components in PSD for single-angle DLS data, whereas WCR method is able to resolve distinctly two components in all cases. Examination of the relative error of peak position shows that WCR method more accurately recovers the peak positions for the single-, 3-, 6- and 10-angle data than the CR method.

From Fig. 1 and 2, we can also find that more accurate recovered distributions were obtained with six angle analysis than other angle analysis.

PSD results obtained for Sample CS (304 nm/600 nm bimodal) are shown in Fig. 3 and Table 5 and it can be seen that both CR and WCR method reliably resolve the two peaks and there is little difference between the two sets of results. For MDLS, we obtain a more accurate PSD and intensity ratio than for single-angle DLS. However, the performance index V is no better for MDLS than single-angle DLS. We observe that single-angle DLS recovers the small particle PSD component well but does poorly with the large particle component. For both analyses the peak positions are determined more accurately when more than one scattering angle is used, further indicating the benefit of MDLS compared with single-angle DLS.

Likewise, the PSD results in Fig. 4 and Table 6 for Sample DS (352 nm/608 nm bimodal) show that both analysis methods perform well. Both peaks are reliably and accurately resolved when more than one scattering angle is used.

Fig. 3 and 4 also indicate that comparing other angle analysis, three angles could give better recovered distributions.

Overall, we can see from the results above that MDLS measurements give more accurate PSD estimations than the single-angle DLS measurements. Furthermore, the proposed WCR method for data inversion and PSD recovery performs better than the un-weighted CR method for Samples AS, BS, CS and DS where PSD peaks are widely separated and large (300 nm, 352 nm) particles are also resolved the two peaks as well as small (112 nm, 200 nm) particles.

4 Experimental data

To evaluate the performance of the WCR method with real experimental data, measurements were made on two bimodal latex sphere mixtures. Standard polystyrene latex particles from Polysciences Inc were diluted into distilled, deionized water and used to prepare the samples. The two stock sphere samples had reported nominal diameters of 306 nm and 974 nm and standard deviations of 8 nm and 10 nm respectively. For Sample AE, the number concentration of the smaller standard was 98.95% and the number concentration of the larger was 1.05%. For Sample BE, the number concentration of the smaller standard was 97.9% and the concentration of the larger was 2.10%. This information can be used to compute the intensity weighting of the measured distribution. The intensity weighting of Sample AE is

50% and 50%. The intensity weighting of sample BE is 34% and 66%.

MDLS measurements were made with a general-purpose laser light-scattering photometer (Brookhaven Instruments, Inc.), fitted with a vertically-polarized He-Ne laser ($\lambda=632.8$ nm), and a digital correlator (model BI-2000 AT). Measurements were made at twelve detection angles ($R=12$): [30°, 40°, 50°, 60°, 70°, 80°, 90°, 100°, 110°, 120°, 130° and 140°]. The angular alignment of the goniometer was checked prior to all measurements. Total measurement times ranged from 200 s to 500 s. All measurements were made with the temperature controlled at 298.15 K.

The experimental data were analyzed using both of CR method and WCR method based on single-angle DLS, 3-angle DLS, 6-angle DLS and 10-angle DLS. Here, CR method is the constrained Tikhonov regularization method. And single-angle DLS was simulated at 90°; 3-angle DLS was simulated at 100°, 120° and 140°; 6-angle DLS was simulated at 30°, 50°, …, 130°; 10-angle DLS was simulated at 30°, 40°, …, 120°. And the values of α were determined using the L-curve method[16]. The values of kk_{θ_r} were estimated using the iterative recursion method for MDLS[7]. Fig. 9 and Fig. 10 respectively show the recovered PSDs for Sample AE and Sample BE for the two analysis methods and different numbers of scattering angle. For Sample AE (intensity ratio ~1∶1) it can be seen from Fig. 5 and Table 7 that both analysis methods resolve two peaks regardless of how many scattering angles are used. For the 3-angle DLS data, a third minor noise peak also appears. Except for the 10-angle data, the WCR method is slightly better at recovering the PSD than the CR method.

Looking at Fig. 6 and Table 8, it can be seen that for Sample BE the recovered PSDs from the MDLS ($M=3$, 6, 10) data clearly showed two peaks using both of WCR and CR method. The recovered PSD from 6-angle DLS appears closer to that expected, and the relative intensity of the peak at large sizes is closer to the true peak intensity ratio of 1.941∶1.000 for WCR method than CR method. However, the recovered PSDs from 1-, 3-, and 10-angle DLS show a third noise peak that was unexpected, although the expected peaks are also recovered except from the from single-angle DLS data. This highlights the problem encountered when noise is mixed in ACF data.

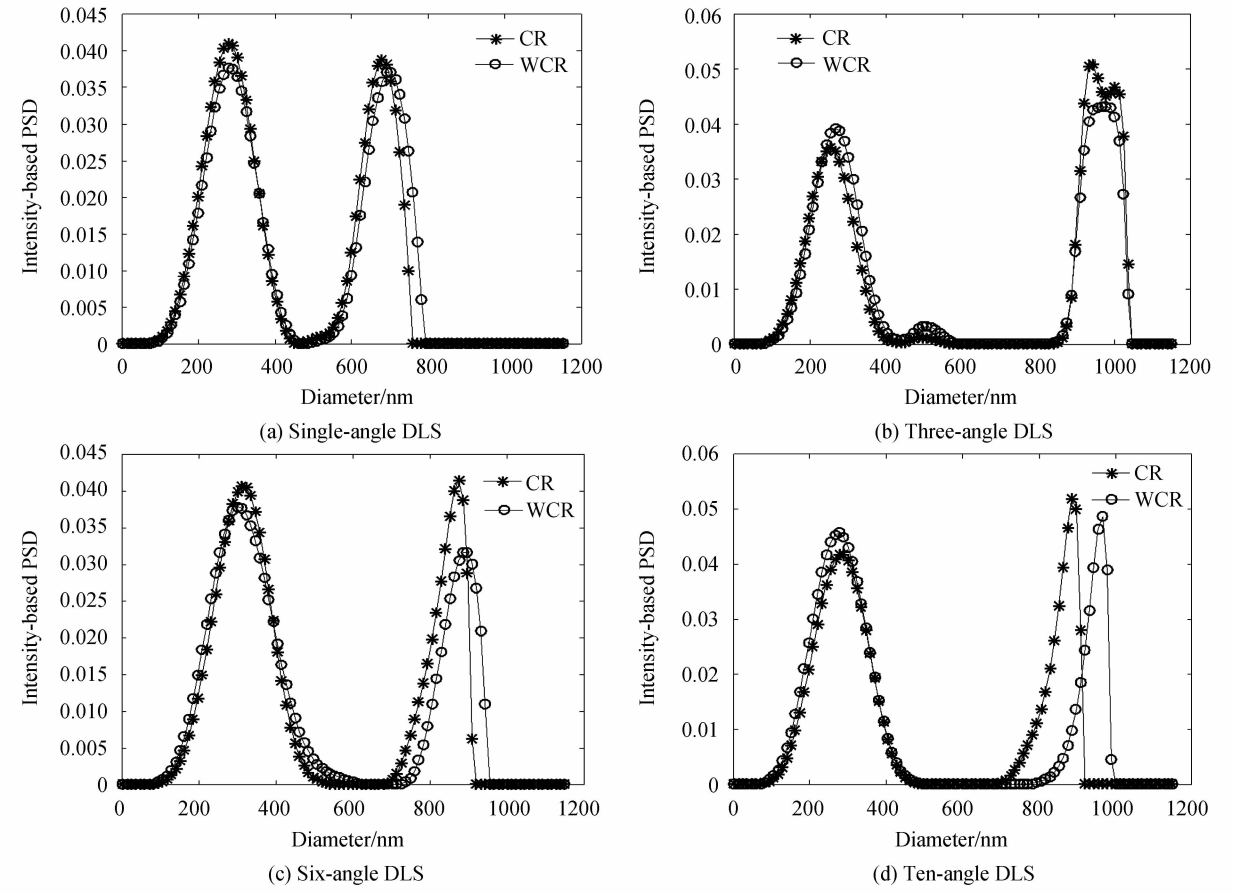

Fig. 5 Intensity-based PSDs recovered from sample AE using CR and WCR method (CR/WCR)

Table 7 Peak position, relative error of peak position, peak intensity ratio and peak area ratio of true and recovered PSDs for sample AE

			Peak position/nm	Relative error of peak position	Intensity ratio	Area ratio
	True PSD		306/974	0.000/0.000	1.000 : 1.000	
Recovered PSDs	1-angle	CR	278/679	0.092/0.303	1.000 : 0.949	1.000 : 0.697
	DLS	WCR	289/702	0.056/0.279	1.000 : 0.987	1.000 : 0.810
	3-angles	CR	255/484/943/1001	0.167/-/0.032/-	1.000 : 0.036 : 1.426 : 1.308	1.000 : 1.161
	DLS	WCR	266/507/978	0.131/-/0.004	1.000 : 0.082 : 1.102	1.000 : 0.866
	6-angles	CR	312/875	0.020/0.102	1.000 : 1.017	1.000 : 0.568
	DLS	WCR	301/886	0.016/0.090	1.000 : 0.836	1.000 : 0.474
	10-angles	CR	289/886	0.056/0.09	1.000 : 1.245	1.000 : 0.581
	DLS	WCR	278/966	0.092/0.008	1.000 : 1.064	1.000 : 0.422

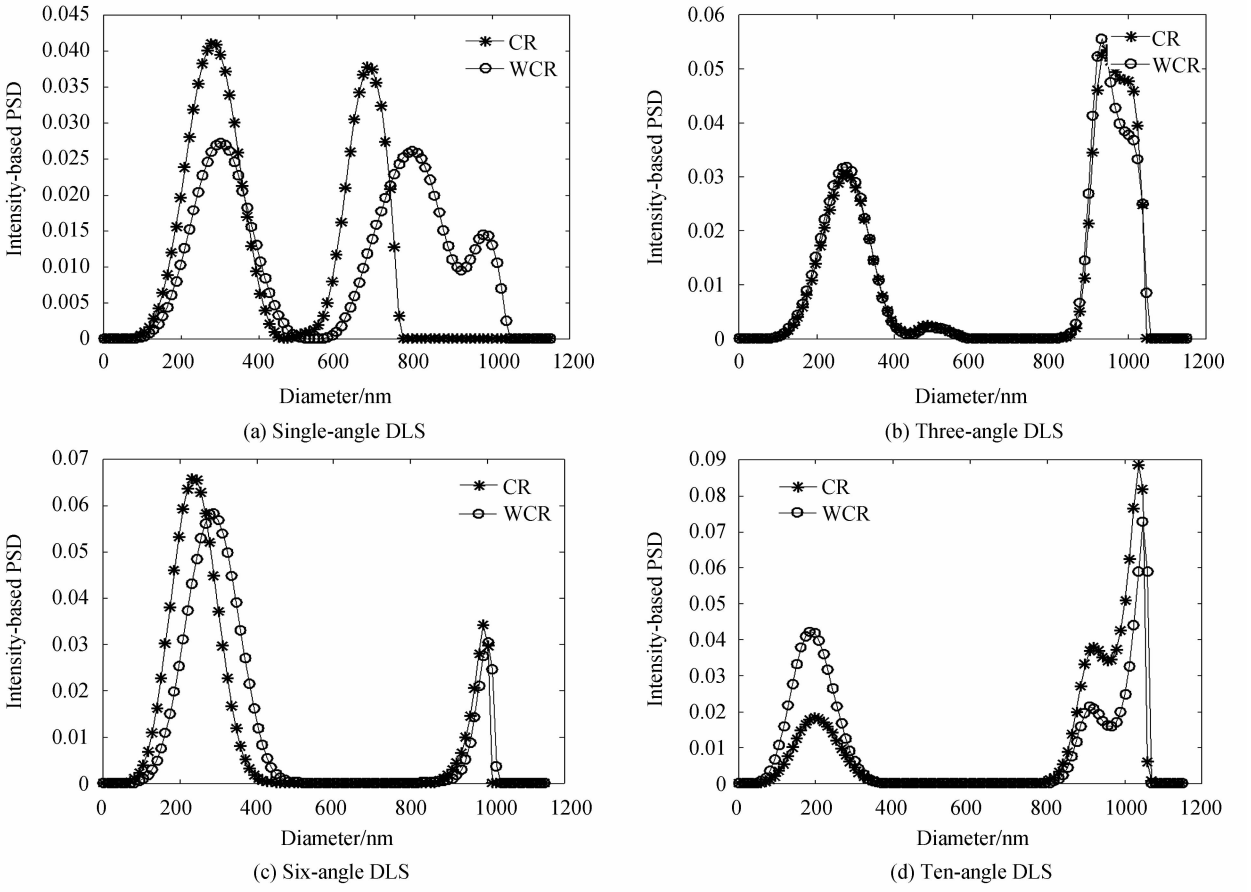

Fig. 6 Intensity-based PSDs recovered from sample BE using CR and WCR method (CR/WCR)

Table 8 Peak position, relative error of peak position, peak intensity ratio and peak area ratio of true and recovered PSDs for sample BE

			Peak position/nm	Relative error of peak position	Intensity ratio	Area ratio
	True PSD			306/974	0.000/0.000	1.000 : 2.000
Recovered PSDs	1-angle	CR	278/679	0.092/0.303	1.000 : 0.920	1.000 : 0.685
	DLS	WCR	301/794/978	0.016/0.185/-	1.000 : 0.956 : 0.535	1.000 : 1.285
	3-angles	CR	278/484/943	0.092/-/0.032	1.000 : 0.083 : 1.757	1.000 : 1.396
	DLS	WCR	279/484/932	0.088/-/0.043	1.000 : 0.070 : 1.742	1.000 : 1.302
	6-angles	CR	232/989	0.242/0.015	1.000 : 0.522	1.000 : 0.183
	DLS	WCR	232/1012	0.241/0.039	1.000 : 0.695	1.000 : 0.214
	10-angles	CR	197/920/1035	0.356/-/0.063	1.000 : 2.068 : 4.831	1.000 : 3.487
	DLS	WCR	208/908/1047	0.320/-/0.075	1.000 : 0.578 : 1.828	1.000 : 1.128

5 Conclusion

We have used MDLS to measure different simulated and experimental bimodal PSDs and used a new

weighted CR method to invert the MDLS data. This method provides more accurate peak positions and peak ratio of intensity contribution than other common inversion methods. There are two main factors contributing to this result. First, MDLS can provide more useful measurement information for the underlying inversion process to recover the bimodal PSD more accurately compared with single-angle DLS. Second, WCR method can reduce the effect of noise in ACF data at large lag time by using weighting while CR method can't. So, WCR data analysis method for MDLS can provide more accurate bimodal PSD recovery than other common methods. Analysis of simulated data show that WCR method can resolve a bimodal PSD with peak position ratio of 1.7, containing large particles (>350 nm) such as 350 nm and 600 nm bimodal particles.

References

[1] CLEMENTI L A, VEGA J R, GUGLIOTTA L M, *et al*. A Bayesian inversion method for estimating the particle size distribution of latexes from multiangle dynamic light scattering measurements[J]. *Chemometrics & Intelligent Laboratory Systems*, 2011, **107**(1): 165-173.

[2] SCHEFFOLD F, SHALKEVICH A, VAVRIN R, *et al*. PCS particle sizing in turbid suspensions: scope and limitations. Particle sizing and characterization[M]. Washington, DC, USA: ACS, 2004: 3-32.

[3] CUMMINS P G, STAPLES E J. Particle size distributions determined by a "multiangle" analysis of photon correlation spectroscopy data[J]. *Langmuir*, 1987, **3**(6): 1109-1113.

[4] BRYANT G, THOMAS J C. Improved particle size distribution measurements using multiangle dynamic light scattering [J]. *Langmuir*, 1995, **11**(7): 2480-2485.

[5] BRYANT G, ABEYNAYAKE C, THOMAS J C. Improved particle size distribution measurements using multiangle dynamic light scattering. 2. refinements and applications[J]. *Langmuir*, 1996, **12**(26): 6224-6228.

[6] VEGA J R, GUGLIOTTA L M, GONZALEZ V D G, *et al*. Latex particle size distribution by dynamic light scattering: novel data processing for multiangle measurements[J]. *Journal of Colloid and Interface Science*, 2003, **261**(1): 74-81.

[7] LIU X, SHEN J, THOMAS J C, *et al*. Multiangle dynamic light scattering analysis using angular intensity weighting determined by iterative recursion[J]. *Applied Optics*, 2012, **51**(7): 846-854.

[8] ZHU X, SHEN J, THOMAS J C. Analysis of noisy dynamic light scattering data using constrained regularization techniques[J]. *Applied Optics*, 2012, **51**(31): 7537-7548.

[9] ZHU X, SHEN J, SONG L. Accurate retrieval of bimodal particle size distribution in dynamic light scattering[J]. *IEEE Photonics Technology Letters*, 2015, **28**(3): 311-314.

[10] THOMAS J C. Photon correlation spectroscopy: technique and instrumentation[C]. Optics, Electro-Optics, and Laser Applications in Science and Engineering, 1991.

[11] BOTT S E, PROVDER T(Ed.). Particle size distribution: assessment and characterization[M]. ACS Symposium Series, 1987.

[12] MIE G. Contributions to the optics of turbid media, especially colloidal metal solutions[J]. *Annalen Der Physik*, 1908, **25**(3): 377-445.

[13] WISCOMBE W J. Improved Mie scattering algorithms[J]. *Applied Optics*, 1980, **19**(9): 1505-1509.

[14] VARGAS-UBERA J, AGUILAR J F, GALE D M. Reconstruction of particle-size distributions from light-scattering patterns using three inversion methods[J]. *Applied Optics*, 2007, **46**(1): 124-132.

[15] YU A B, STANDISH N. A study of particle size distribution[J]. *Powder Technology*, 1990, **62**(2): 101-118.

[16] HANSEN P C, O'LEARY D P. The use of the *L*-curve in the regularization of discrete II-posed problems[J]. *Siam Journal on Scientific Computing*, 1993, **14**(6): 1487-1503.